ISSN 0742-0463, Journal of Volcanology and Seismology, 2025, Vol. 19, No. 4, pp. 303–318. © Pleiades Publishing, Ltd., 2025.

Magmatic Activity of Mutnovsky Volcano and the Formation of a Crater at the Place of the Blowing Well 022

A. V. Kiryukhin[a], *, A. Yu. Polyakov[a], A. V. Sergeeva[a], I. A. Nuzhdaev[a], N. B. Zhuravlev[a], P. O. Voronin[a], O. O. Usacheva[a], and M. Yu. Puzankov[a]

[a] *Institute of Volcanology and Seismology, Far East Branch, Russian Academy of Sciences, bulvar Piipa 9, Petropavlovsk-Kamchatsky, 683006 Russia*

**e-mail: AVKiryukhin2@mail.ru*

Received November 25, 2024; revised February 25, 2025; accepted May 12, 2025

Abstract—Mutnovsky Volcano is characterized by predominantly magmatic activity for the last 4 thousand years in the northern sector where the Mutnovsky geothermal field lies. Magmatic activity is identified using the Frac-Digger method based on seismic data as reported by the KB FRC UGS RAS. The most significant sequence of shallow dikes striking northeast has been manifested at the surface by blowing two-phase geothermal wells. Dike emplacement in March 2024 was synchronized with a hydrothermal explosion producing a crater of volume reaching 0.36 million m^3 at the place of well 022 (Crater 022+). Unaltered fragments due to the explosion indicate a lithoclastic character in the gas-enriched head of the dike. The bottom of the explosion crater is a hydrothermally altered (opal, zeolite) 160×75 m^2 in area. The mechanism of the hydrothermal explosion is treated as resulting from hydraulic fracturing by means of a shallow dike, with subsequent increase in pressure in the shallow geothermal reservoir near the well with a closed wellhead control-valve.

Keywords: hydrothermal explosion, dike, Mutnovsky Volcano, magma, well

DOI: 10.1134/S0742046325700216

1. INTRODUCTION

The magmatic activity of Mutnovsky Volcano is marked at the ground surface of the northern base of the volcano by a chain of large geothermal fields and discharges of thermal springs. The seismic stations operated by the KB FRC UGS RAS and the geothermal wells of the Mutnovsky geothermal field in operation at present supply information for assessing the dynamics of the volcano's magmatic activity. It is owing to this that the North Mutnovsky volcano-tectonic zone (which is also the zone of magmatic activity of Mutnovsky Volcano) has been during 15 years an underground laboratory to study the mechanisms of the transport of magmatic fluids and creating natural hydrothermal circulation systems in the hydraulic fracture mode.

The magmatic activity of active volcanoes occurs in the form of dikes and sills due to hydraulic fracture of host rocks, which takes place perpendicularly to the minimum effective stress (Gudmundsson, 2022) The process generates strike slip faults and micro-earthquakes (MEQ) of various types, which enables identification of 3D geometry of magma injections on a volcano in real time (Kiryukhin et al., 2016, 2018, 2022; Kiryukhin, 2020), but most dikes (over 99%) do not reach the ground surface and remain underground as "arrested dikes" in the terminology of Gudmundsson (2006). The rare cases in which a dike reaches the ground surface (or approaches it) outside the contour of the volcano's main vent are accompanied by lateral lava effusions (or by hydrothermal explosions).

The hydrothermal explosion (magma-phreatic, phreatic eruption) is a 3D failure in the near-surface rock layer as the gas pressure increases (one particular case involves steam) at its bottom above the rock pressure (the vertical stress). A hydrothermal explosion can be excited by the following causes: (1) contact of magma and water with subsequent conversion of the latter from liquid to gaseous phase, decreasing vertical gradient of fluid pressure and increasing pressure in the near-ground layer; 2) a decrease in piezometric level toward the zone of higher temperatures with a thermal hydrodynamic effect similar to that described above. Examples of hydrothermal eruptions are described in numerous publications; one of the more complete is (Browne et al., 2001).

Hydrothermal explosions within productive geothermal fields pose hazard to the infrastructure of geothermal electric power stations, productive wells and pipelines of heat-carrying fluid. As an example, the Onikobe GPP (geothermal power plant) in Japan has been operated since 1975 (15 MW of electrical energy). According to Akasaka et al. (2015), thermal springs began to discharge near well 128 on September 8, 2010; the discharge was gradually increasing to become fumarolic activity. A hydrothermal explosion occurred on October 17, 2010 hurling material to heights reaching 450 m and producing a crater 45 m across. The result was for well 128 to collapse into the crater, 2 people were killed, and in addition wells 136 and 138 have been damaged. An analysis of water from the crater (sampled from on board a radio-controlled helicopter) showed that this water was identical with that from well 128, indicating that the column fracture in the well has caused accumulation of high pressure steam in the near-surface zone with a subsequent explosion. To stop steam and gas discharges, two inclined directed wells were drilled. The wells have penetrated the damaged wells 128 and 138, cement was injected to stop the steam–gas eruption, and the crater was filled with cold water (April 18, 2014).

An eruption of magma was recorded to occur in 1975 from a geothermal well at the Krafla geothermal field, Iceland which is characterized by high magmatic activity, with magma flowing laterally for distances reaching 50 km (Stefansson, 1981).

At the same geothermal field in the Krafla Caldera, Iceland, well IDDP-1 was drilled to a depth of 2.1 km in 2008–2009. This well reached a magma body (sill) whose temperature was above 900°C (Fridleifsson et al., 2015). A pilot extraction of heat-carrying fluid was performed (two years, March 2010 through July 2012) after intensive cooling with the formation of a permeable zone due to the creation of thermally induced cooling cracking in a crystallized magma (300 thousand m^3 of cold water was injected during drilling) and subsequent recovery of temperature. These tests showed that well IDDP-1 could be operated to yield 40–50 kg/s at wellhead pressure 40–80 bars (overheated steam with enthalpy 3200 kJ/kg), maximum wellhead temperature 450°C, and pressure 140 bars. This corresponds to the yield of 25–35 MWe, but stable operation requires solving the problem of cleaning the steam from SiO_2 (62 ppm), HCl (100 ppm), and S. The casing of well IDDP-1: conductor 13-3/8" inside which is a production column (9-5/8") down to depth 1950 m, then to depth 2072 m is the filtering column 9-5/8", then in the interval 2072–2096 m is an open hole 12 ¼". Tracer testing showed the presence of a hydraulic connection between IDDP-1 and production wells at the Krafla field, which essentially implements a magmatic circulation system for extracting the heat-carrying fluid. A failure of the wellhead control-valve occurred at well IDDP-1 in 2012, and the production column was fractured during injection of cold water. Hence it was decided to "suppress" it with cold water, and afterwards to abandon.

Well 022 (wellhead elevation was +702 m) at the Mutnovsky geothermal field was drilled in 1988 to a depth of 1532 m (Asaulova, 1994[1]). The well structure: the conductor 324 mm to depth 242.5 m, production column 245 mm from 5 m to 700.5 m, production column 168 mm from 595 m to 1197 m, filtering column 127 mm from 1149 m to 1529 m. After the drilling was over, the bottom-hole temperature was 300°C (as recorded by geothermometers), the bottom-hole pressure was 102.9 bars (the water level in the well was ≈500 m below wellhead). Well 022 was operated in the uncontrolled flowing mode until 2021 (Fig. 1a); in 2022 the wellhead control-valve was closed (see Fig. 1b), and the wellhead pressure was 25.5 bars based on the temperature of saturated steam 225°C measurements (see Fig. 1c).

A powerful natural hydrothermal explosion of well 022 at the Mutnovsky geothermal field occurred in March 2024 (see below), producing a crater of volume 0.36 km^3 at the place of the well 022 head. The explosion was preceded by smaller hydrothermal explosions near that same well in the spring of 2003 (Melnikov, 2004; Kiryukhin et al., 2010, 2014) and in the spring of 2023. For this reason the latter crater due to the hydrothermal explosion at the place of well 022 will be named *Crater 022+*.

The goal of the present paper is to describe the magmatic and production activity preceding the formation of Crater 022+ and accompanying geochemical changes in the regime of the productive geothermal reservoir, as well as to estimate the parameters and to develop the mechanism of the 2024 hydrothermal explosion in relation to the magmatic activity of Mutnovsky Volcano and the production history of the Mutnovsky geothermal field.

2. THE GEOLOGICAL STRUCTURE AND MAGMATIC ACTIVITY OF MUTNOVSKY VOLCANO

The geological structure, hydrogeological conditions, and the distribution of hydrothermal discharges in the Mutnovsky geothermal area are described in (Vakin et al., 1986, Kiryukhin, 1993, Selyangin, 1993). The main geological units of the Mutnovsky geothermal area reached by wells or exposed at the ground surface are as follows: (1) Miocene sandstones and Paleogene–Neogene volcanogenic-sedimentary deposits; (2) Miocene diorite intrusions; (3) Pliocene dacitic and rhyolitic tuffs and lavas; (4) Pliocene–Quaternary basalts and andesitic tuffs and lavas; (5) the cones of volcanoes: Mutnovsky-1, Mutnovsky-2,

[1] *Asaulova, N.P., Report on the Results of Preliminary Exploration of Testing Sites for reinjection of waste fluid at the Mutnovsky Geothermal Field (1988–1993)* (in 2 books), village of Termalnyi, Kamchatka Region, 1994.

Fig. 1. The blowing well 022 in the southeastern flank of the Mutnovsky geothermal field (for the location of the well see Fig. 2), in the background is a layer of "silicate snow" (see subsection 4.4), considerable decreases in two-phase blowing wellhead temperature (down to 85°C at atmospheric pressure) were observed there since 2019, the photograph was made in 2020 (a); (b) well 022 after closing the control valve in 2022; (c) head of well 022 with measured temperature 225°C.

Mutnovsky-3, and Mutnovsky-4; (6) Upper Pleistocene and Holocene andesites and basalts; (7) extrusions of Upper Pleistocene rhyolites.

These geological units existing in the Mutnovsky productive reservoir are defined as follows (Kiryukhin, 1993, 1996): (1) Miocene sandstones (N_{1-2} as_1); (2) diorite intrusions (δN_{1-2}) (dikes crossed by wells 04, 011, and 012); (3) contact zone of Miocene intrusions (N_1br); (4) Miocene tuffs and lavas (N_{1-2} as_2); (5) Pliocene rhyolitic tuffs (N al_1); (6) Pliocene lavas (N al_2); (7) Quaternary ignimbrites, tuffs and lavas, rhyolite–dacite extrusions.

Mutnovsky Volcano is a complex of four volcanic cones (M1, M2, M3, and M4) that have been persistently active since the Late Pleistocene (Fig. 2). The chronology of the volcano's eruptions was reviewed by Selyangin (1993) as follows. Mutnovsky-1 (the oldest of the four) was active some 60–80 kY ago B.P. Mutnovsky-1 has formed basaltic, basaltic andesite, andesitic, and dacitic lavas and pyroclastic rocks whose total volume is about 58 km^3. At present one can see in the northeastern sector of the Kleshnya Range an exposed complex of basaltic dikes striking nearly north–south, which are treated as the eroded part of the plumbing system supplying Mutnovsky-1. The volcano Mutnovsky-2 functioned 30–40 kY ago B.P., its center was 3 km southeast of the center of Mutnovsky-1, Mutnovsky-2 has discharged about 24 km^3 of lava and pyroclastic material. The composition of the volcanic rocks of Mutnovsky-2 varies between basalts and dacites, and shows an overall similarity to Mutnovsky-1. Mutnovsky-3 stands between Mutnovsky-1 and Mutnovsky-2 and has a relatively small volume of volcanic rocks (~5 km^3).

Mutnovsky-3 is composed of alternating pyroclastic and lava flows with parasitic cones along the periphery, which is also typical of Mutnovsky-1 and Mutnovsky-2. Mutnovsky-3 is pierced by basaltic dikes, and its central part is composed of hydrothermally altered rocks. The composition of the Mutnovsky-3 volcanic rocks varies between basalts and rhyodacites. The Mutnovsky-3 summit caldera is 1.5 × 2.0 km in size (see Fig. 2). It was formed by an eruption discharging 2.0–2.5 km^3 pumice, and part of the caldera is at present filled with a glacier (2.5 km^2) and with lava flows discharged by Mutnovsky-4. Mut-

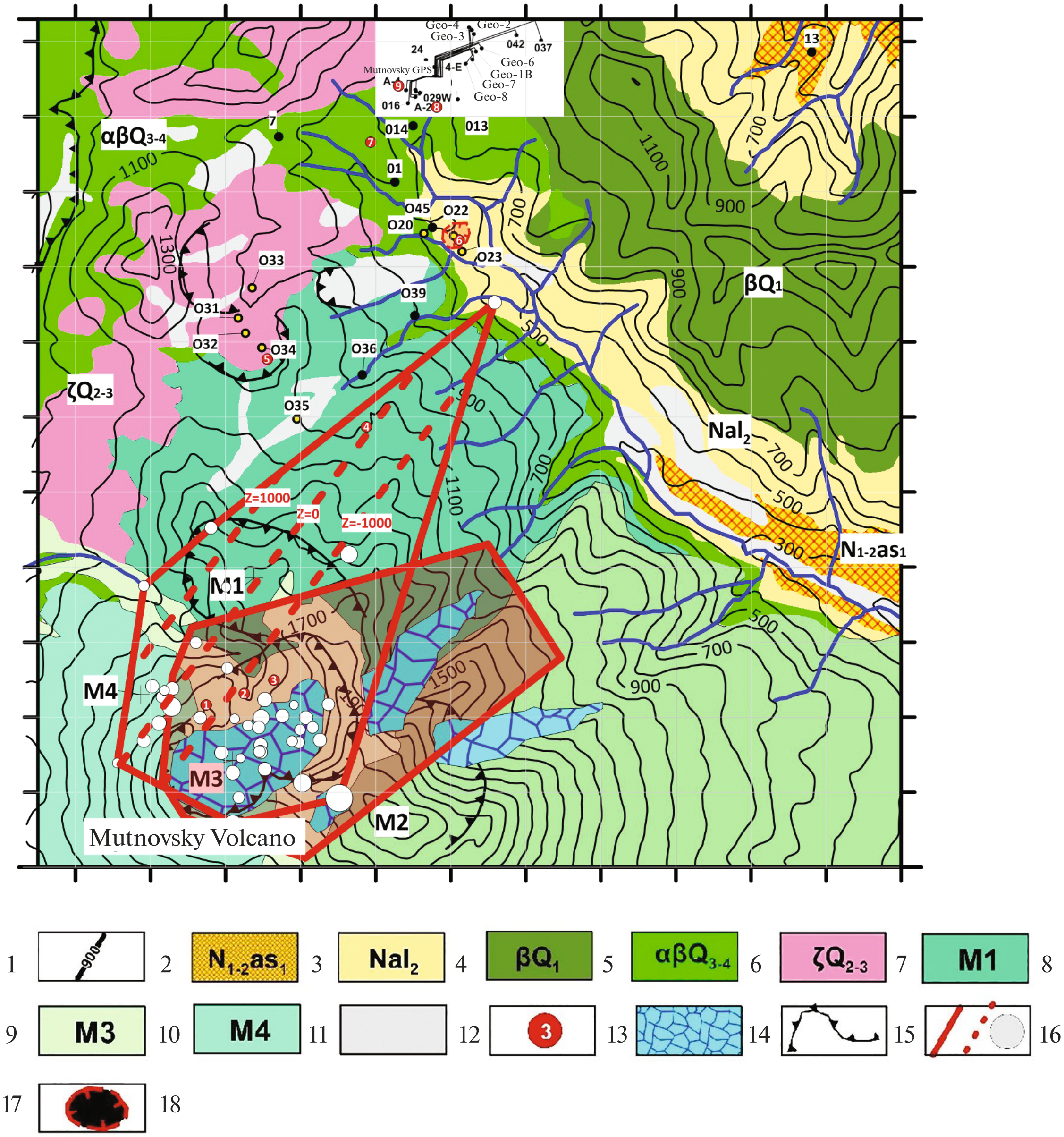

Fig. 2. A schematic geological map and the relief of the Mutnovsky geothermal area. The tick marks are at intervals of 1 km. Legend: (1) wells (accidentally blowing wells are marked by yellow inner circles); (2) isolines of topographic surface, m; (3) Miocene sandstones (N_{1-2} as_1) and diorite intrusions (δN_{1-2}); (4) Pliocene lavas (N al_2); (5) Pliocene-Quaternary basalts and andesitic tuffs and lavas (Zhirovskoi Volcano) (βQ_1); (6) Upper Pleistocene and Holocene andesites and basalts ($\alpha\beta Q_{3-4}$); (7) Middle and Upper Pleistocene rhyolite extrusions ζQ_{2-3}; (8, 9, 10, 11) M1, M2, M3, M4 denote Mutnovsky-1, Mutnovsky-2, Mutnovsky-3, and Mutnovsky-4 volcanoes (after Selyangin, 1993); (12) fluvioglacial deposits (Q_4); (13) thermal occurrences (fumarolic fields): (1) Active Crater, (2) Bottom Field, (3) Upper Field, (4, 5) North Mutnovsky (Eastern and Western), (6) Novye-2003 (Crater 022+), (7) Dachnye (Active group), (8) Radon spring, (9) Medvezhy; (14) glaciers in the crater of Mutnovsky Volcano; (15) volcanic craters, craters due to phreatomagmatic explosions; (16) dike #178 (exploding Crater 022+): map-view contours (solid lines), traces (dashed lines) at elevations −1000 m, 0 m, +1000 m, and the epicenters of accompanying MEQs (microearthquakes, circles are proportional to magnitude); (17) sill #177 (preceding to dike that exploded Crater 022+): sill contour is shown by a colored polygon; (18) Crater 022+. Note. The inset at top of figure shows productive wells supplying fluid to the Mutnovsky GPP.

novsky-3 also contains an intracaldera basalt–andesite cone and a rhyodacite extrusion. The end of Mutnovsky-3 activity is recorded by the extrusion of a dacite dome whose age is estimated approximately as 4000 years based on local tephrostratigraphic data (Selyangin, 1993).

Mutnovsky-4 is the youngest volcano in the Mutnovsky volcanic complex, its age is estimated approximately as 11 kY ago (Selyangin, 1993). Mutnovsky-4 stands 1 km southwest of Mutnovsky-3, its total volume is estimated as 3.8 km^3. Mutnovsky-4 is com-

Table 1. The geometrical characteristics of dikes and sills in March 2024 which preceded the hydrothermal explosion of well 022 in April 2024

#	Dip angle, °	Dip azimuth, °	*X*, m	*Y*, m	*Z*, m	Date	Ks max	##
177	15.4	89.1	43417	14790	−2340	4 Mar. 24	4.2	463
178	58.4	126.7	43268	15163	−1408	4 Mar. 24	4.3	42
179	48.6	151	43565	14944	−2508	21 Mar. 24	4.8	152

means identification number of a dike or a sill, ## the number of MEQ hypocenters that have formed a plane-oriented cluster of magma injection.

posed of basaltic andesite lavas and pyroclastic flows. We can thus state that the activity of Mutnovsky Volcano has changed during the last 30 kY ago from effusive–pyroclastic to magmatic.

3. THE 2009–2024 MAGMATIC ACTIVITY OF MUTNOVSKY VOLCANO BASED ON SEISMIC DATA

In the present study we are using the Frac-Digger method (Kiryukhin and Kiryukhin, 2016) to identify injections of dikes and sills beneath Mutnovsky from seismic data. The idea of the method consists in identifying plane-oriented clusters of earthquake hypocenters in a specified time interval. A new element (seismic event) can be incorporated into a cluster using the following criteria: (1) the time difference (δt); (2) the distance difference in the horizontal plane (δR); and (3) the requirement of nearly plane orientation (i.e., the distance from the event to the fitting plane (δZ)). The identified features are treated as magma injections in the form of dikes or sills. A description and substantiation of the method's applicability can be found in the monograph (Kiryukhin, 2020), as well as in publications dealing with its practical uses to study Klyuchevskoi, Bezymyanny, Plosky Tolbachik, Mutnovsky, Koryaksky, and Avachinsky volcanoes (Kiryukhin et al., 2016, 2017, 2020, 2022, 2023a).

Seismicity was recorded by five seismic stations operated by the KB GS RAS since 2009 (MTV, GRL, ASA, RUS, and PET). From September 2024 onward the number of seismic stations in the Mutnovsky geothermal area has been increased by adding three more: DVGB, KLDG, and VKN (Dvugorbaya, Gorelyi caldera, and Vakin).

The result was to find that magma injections occur under NE–SW horizontal compression, producing dikes and sills mostly at absolute depths of –4 km to –2 km; the dikes dip southeast at angles of 20 to 50 degrees (this direction is identical with the orinetation of productive faults at the Mutnovsky geothermal field), at depth –3 km a zone of sill injection is hypothesized with area 62 km^2, shifted N-NE from the crater of Mutnovsky Volcano. A total of 190 magma injections have been identified for the period 2009 through August 2024.

The most significant magma injections which occurred in 2024 took place in March. The characteristics of the features identified using the Frac-Digger method (the criteria of identification were δt = 30 days, δR = 12 km, δZ = 1 km, N = 6), namely, a sill (#177) and two dikes (#178, #179), are listed in Table 1 and shown in Figs. 2 and 3. Sill #177 with dimensions 5 × 2 km was formed beneath the Mutnovsky-3 crater at a depth of 2.3 km with a NE shift of 3 km; it was recorded by 463 MEQs (the maximum magnitude was M = 1.35, M = 0.5Ks–0.75). Simultaneously, dike #178 was injected, upwards (the depth range above –2 km) and in the N–NE direction; it was recorded by 42 MEQs (the maximum magnitude was M = 1.4). The strike and dip of dike #178 are similar to the characteristics of the Main productive fault (Kiryukhin et al., 2010), as well as to those of a series of identified dikes (116, 30, 52, 111, 62, 66) with the numbers of MEQs over 30 (see Fig. 10 in the paper (Kiryukhin et al., 2022)). In the end of March, dike #179 was also injected; it had an orientation similar to that of dike #178, but in the opposite direction.

We also wish to note that the seismic station MTV had gaps of recording because of severe climatic conditions (April–June 2022, January 2023, January–February 2024), which might have caused missed episodes in the magmatic activity of Mutnovsky Volcano during the time intervals indicated.

4. GEOCHEMICAL INDICATORS OF MAGMATIC ACTIVITY IN THE AREA OF CRATER 022+

4.1. Inflows of Magmatic Gas

Electrical energy at the Mutnovsky power station is generated by two turbines 25 MW each, steam is supplied to the turbines from geothermal wells A2, A4, Geo-1B, Geo-2, Geo-3, Geo-4, Geo-6, Geo-7, Geo-8, 029W, 016, GK1, 042, 037 (see Fig. 2, data for 2024) through two separators. The measurement of partial pressure of uncondensing gases (P ncg) at the condenser of the Mutnovsky power station allows tracking inflows of magmatic gas synchronized with magma injections at Mutnovsky Volcano (Kiryukhin et al., 2022). With this end in view, an original device was developed and tested in 2019 to provide for remote

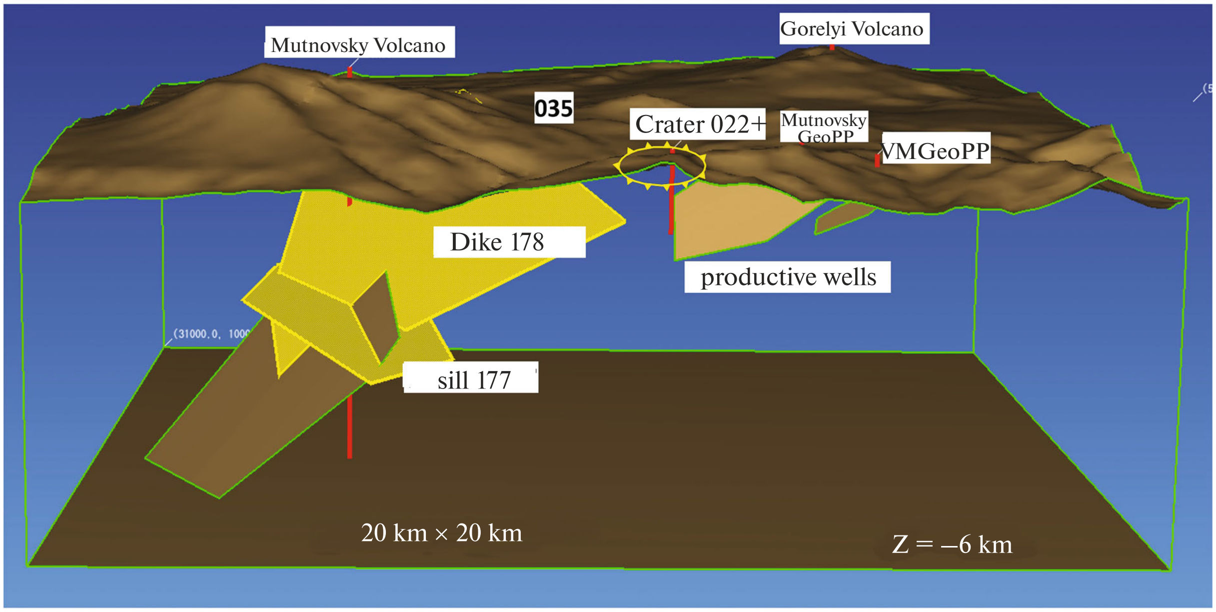

Fig. 3. The sequence of dike and sill injections in March 2024 before the hydrothermal explosion at well 022 in April 2024. The figure also shows productive faults that have been confirmed by drilling of trial boreholes.

observations of P ncg changes in geothermal steam in real time mode (Patent no. 2801789 C1, Kiryukhin et al., 2023a). Since 2020, the branch *Vozobnovlyaemaya Energiya* of *Kamchatskenergo* PJSC provides original data for calculating and monitoring P ncg. In the first half of 2024, four significant anomalies in P ncg were recorded, the largest being anomaly with amplitude P ncg = 0.5 bars as of March 27, 2024 (Polyakov and Kiryukhin, 2024). This anomaly was synchronized with the injection of dike 178 which initiated the hydrothermal explosion and the formation of Crater 022+.

4.2. Geothermometers, Gas Composition of the Wells in the Near-Dike Zone

Another source of information on the magma injections in the northeastern sector of Mutnovsky Volcano is supplied by accidentlally blowing wells at the foothills of Mutnovsky Volcano (035, 020, 022 etc., see Fig. 2). These wells are situated near the epicenter of the zone of magma injections, or the intersection between the topographic surface and the averaged plane representing the dike series striking northeast (see Fig. 2). The annual discrete sampling of gas and hydrochemical material and measurements of wellhead temperature during the period 2015–2024 (Tables 2 and 3) show the following: (1) the Na–K geothermometer (Fournier, 1981) gave water temperature in the range between 254 and 366°C (well 035) and between 270 and 353°C (well 022); (2) the wells are blowing gas-enriched fluids (the gas/water ratio being between 0.1 and 600 L/kg), the gas component is largely of atmospheric origin. The high concentration of gas produces unbearable noise around the wells (well 022 produces noise at 110–115 dB and well 035 at 120–125 dB with going off scale at 130 dB (sound level meter DT-85A)), as well as considerably diminishing the saturation temperature at wellheads (77°C at atmospheric pressure at the head of well 035 and 85°C at the head of well 035), a transparent flow at wellhead indicates gas-dominated discharge; (3) judging from the bulk gas composition, wells 022 and 035 operated mostly because of heated atmospheric air, while some samples show signs of magmatic CO_2 and thermogenic CH_4 as inferred from the isotopic composition of carbon. It is supposed that atmospheric air is heated by magma intrusions in zones of incomplete water saturation (the depth range above +200 m abs. for the Mutnovsky geothermal field area); (4) the isotopic composition of water is in agreement with meteoric water from a height of about 1000 m. We can thus assert that accidentally blowing wells record an active fissure zone of dike injection, produce an air-meteoric steam–gas mixture with a basic temperature of about 250–300°C from its gas-charged litho-clastic head part. A gas sample taken on August 12, 2017 at well 035 seems to have been enriched in magmatic CO_2, which can be sybchronized with a dike injection in an immediate vicinity of the well.

After the formation of Crater 022+, well 035 appreciably decreased in productivity, and became less noisy, the concentrations of main chemical macrocomponents decreasing. This probably was due to the opening of the host dike fissure (on the extension of which are both well 022 and well 035, see Fig. 2) and to increased inflow of cold meteoric water into it. The

Table 2. The chemical and isotopic compositions of water in fluids at the Mutnovsky blowing geothermal wells at the base of Mutnovsky Volcano

Well no.	Date	pH	HCO_3^-	SO_4^{2-}	Cl^-	NH_4^+	Na^+	K^+	Ca^{2+}	Mg^{2+}	HBO_3	SiO_2	T Na–K	$TSiO_2$	δD‰	δ¹⁸O‰
022*	13 Aug. 2007	3.7		269	300	15	211	41	14	26	155	845	274	305		
022	17 Aug. 2015	8.9	93	96	298	0	230	71	1	0	152	391	352			
022	13 Sep. 2016	7.3	37	40	70	23	48	11	0	0	18	389	298		–109.4	–14.9
022	13 Aug. 2017	6.9		37	64	15	52	10		<0.1	28	220	271		–107.2	–15.6
022	9 Aug. 2018	8.6	104	20	4		64	0	5	0	2	15		53	–101.5	–12.8
022	7 Aug. 2019	4.4	<1.0	274	192	5	193	62	2	<0.1	132	139	360	157		
022	11 Aug. 2020	6	77	91	251	6	173	40	2	<0.1	119	1075	300	333		
022	8 Aug. 2021	7.7	57	115	234	6	186	37	1	<0.1	75	156	276	164	–99.0	–12.0
022*	8 Aug. 2023	3.2		272	287	40	204	43	29	4	188	608	283	271		
022*	26 Sep. 2024	7.9	91	420	280	4	308	37	73	4	140	341	207	220		
022*	26 Sep. 2024	8	96	308	279	0	262	39	78	3	144	275	235	203		
020	10 Aug. 2024	6.6	53	95	214	7	175	46	1	<0.1	150	552	320	262		
035	17 Aug. 2016	5.5	1	87	7	13	23	6	6	1	57	323	321	215	–103.4	–13.1
035	12 Aug. 2017	4.4		48	21	6	33	6		<0.1	31	187	262	176	–101.0	–14.6
035	10 Aug. 2018	7.3	10	52	12	6	24	7	2	1	58	211	328	184	–104.0	–12.8
035	10 Aug. 2019	4	<1.0	13	52	6	25	8	1	<0.1	180	180	360	173		
035	15 Sep. 2020	6.9	17	14	5	11	7	2	<5	<0.1	29	67	337	116	–112.0	–15.2
035	6 Aug. 2021	7.6	9	48	7	10	16	3	<5	<0.1	19	183	267	174	–103.0	–13.0
035	10 Aug. 2022	5.6	10	30	4	8	7	2	1	<0.1	22	189	318	176		
035	5 Aug. 2023	7.1	23	34	<10		14	4	1	<0.1	25	146	344	160		
035	8 Aug. 2024	6.2	16	14	10	11	6	3	1	<0.1	14	31	505	81		

Wells were sampled by A.V. Kiryukhin, A.Yu. Polyakov, P.O. Voronin, N.B. Zhuravlev, A.V. Sergeeva, and L. Pozolotina. The chemical analysis was performed at AC IVS FEB RAS. The isotopic analysis of water (2016–2018 samples) was performed by P.O. Voronin using LGR IWA 35EP at IVS FEB RAS, the isotopic analysis of water (2020–2024 samples) was performed by I.V. Tokarev at RC XRDMA of the St. Petersburg University Science Park using a Picarro L2120-i laser infrared spectrometer.

* Samples were taken from the creeks that drain the explosion craters of well 022.

Table 3. The composition of gas (vol %) and the isotopic composition of carbon in blowing geothermal wells of the Mutnovsky field at the base of Mutnovsky Volcano, R is gas content L/kg

Well no.	Date	T, °C	H_2	Ar	O_2	N_2	CO_2	CH_4	$\delta^{13}C$, ‰ (CH_4)	$\delta^{13}C$, ‰ (CO_2)	R, L/kg
022	13 Sep. 2016	107		1.00	22.10	69.00	4.45	0.00		−7.8	
022	13 Aug. 2017	121	n.d.		19.94	78.01	1.09	0.01			
022	9 Sep. 2018	128	0.00	0.10	1.49	96.80	1.69	0.00	−22.1		3
022	7 Aug. 2019	95	0.01	0.95	15.21	80.29	3.50	0.04			0.1
022	11 Aug. 2020	91	0.28	0.75	18.0	77.8	3.1	0.1		−14.1	8
022	8 Aug. 2021	85	0.1	0.79	18.8	78.6	1.8	0.03		−14.6	
022	11 Aug. 2022	225									
020	10 Aug. 2024	94	0.05	0.86	20.5	77.6	0.92	0.01			30
035	17 Aug. 2016	>100	0.02	0.80	21.30	73.80	0.64	0.00			
035	12 Aug. 2017	48	4.75		0.20	5.33	88.5	0.94		−6.9	
035	10 Aug. 2018	98	0.01	0.72	18.76	79.29	1.23	0.01	−19.8		
035	10 Aug. 2019	80	0.01	0.90	19.57	78.33	1.18	0.01			
035	11 Aug. 2019	80	0.02	0.91	19.72	78.51	0.84	0.01			600
035	8 Aug. 2020	81	0.04	0.80	18.7	79.7	0.76	0.01		−27.8	
035	14 Sep. 2020	81	0.16	0.83	17.8	79.6	1.5	0.05		−25.0	
035	6 Aug. 2021	80	0.004	0.76	18.7	79.4	1.2	0.003		−23.3	
035	10 Aug. 2022	72	0.08	0.81	19.8	78.6	0.69	0.007		−2.7	30
035	5 Aug. 2023	79	0.04	0.75	20.5	78.2	0.48	0.002		−20.9	4.5
035	8 Aug. 2024	77	0.05	0.80	20.5	77.9	0.92	0.003			27

The wells were sampled by A.V. Kiryukhin, A.Yu. Polyakov, P.O. Voronin, N.B. Zhuravlev, A.V. Sergeeva, and L. Pozolotina. The chemical analysis was performed at AC IVS FEB RAS. The isotopic analysis ($\delta^{13}C$) was performed by B.G. Pokrovsky (GIN RAS).
Well 022 was closed on August 11, 2022, the wellhead pressure corresponding to temperature 225°C is at least 25.5 bars. n.d. means not determined.

heir (for sampling) to the exploded well 022 was the nearby blowing well 020, which is characterized by a similar chemical and gas composition.

4.3. Mineralogical Indicators of Hydrothermal Activity in Crater 022+

The bottom of the crater produced by explosion of well 022 rapidly formed deposits of a complex composition. They were seen as white and yellow crusts, heated patches in the crater were covered by salt efflorescence. Samples from the deposits in the central part of the crater were studied by X-ray diffractometry and infrared spectroscopy. The diffractograms were recorded using an XRD MAX 7000 X-ray diffractometer (Shimadzu) in the range 5°–70° 2θ, at a step of 0.1° 2θ, the scanning rate was 2 deg/min, which is equivalent to exposure at the point 3 s. The infrared spectra were recorded using an IR-Affinity-1 infrared spectrometer (Shimadzu), in the range 400–4000 cm^{-1}, resolution 4 cm^{-1}, the number of scans was 100. Samples were prepared for recording by pulverizing them along with potassium bromide in an agate mortar and pressurized to obtain tablets. The next step was to record absorption spectra.

The mineral composition of the deposits that were accumulated in the bottom of the explosion crater is complex (Fig. 4). The main mineral is gypsum; in addition, associating with are found minerals of the jarosite group, ferricopiapite, sulfur, zeolites that are similar to stilbite, feldspars, halite, amorphous hydrates of aluminum sulfate and siliceous deposits. The composition of the mineral association divides into two components, with the one including amorphous silica, zeolites, and sodium chloride. These components were formed under the influence of deep alkaline chloride–sodium waters, as has been previously established for the Pauzhetka siliceous blankets at well outlets (Sergeeva et al., 2024). The other part, iron sulfates, sulfur, and gypsum, are more characteristic of present-day geothermal fields showing violent steam–gas activity.

The explosion seems to have occurred in a reservoir containing alkaline waters where siliceous deposits which consisted of amorphous hydrated silica (opal), poorly crystallized zeolites, and probably gypsum began to form. Gypsum as such can form in a wide

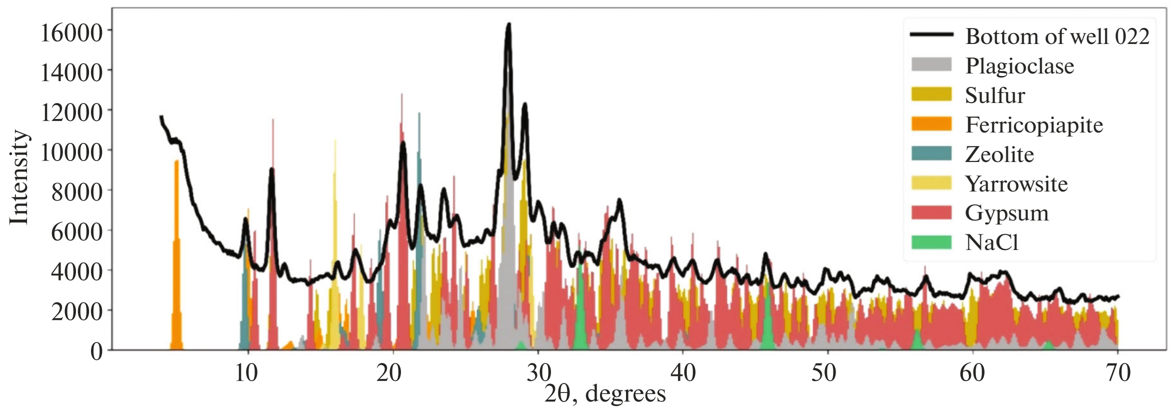

Fig. 4. A diffractogram of the deposits sampled from the bottom of the crater produced by the explosion of well 022.

range of pH. Before the explosion, the environs of well 022 were covered with a layer of amorphous silicate deposits (Table 4) which have been called "silicate snow" for their appearance of a snow cover (see Fig. 1). These deposits took many years to form due to free well blowing a steam-water mixture with a higher concentration of silica. Silica dissolution was favored by high temperature in the reservoir and an alkaline environment of discharging solutions. As the aerosol was cooling and the water evaporating, silica particles were deposited on the ground. The explosive events were also followed by the formation of siliceous deposits, but the changes in the discharging fluid have also changed the mineral association.

The appearance of minerals that are characteristic of active thermal fields can be due to leaching of rock-forming minerals by products from oxidation of sulfur-bearing compounds. The penetration of aqueous solutions of meteoric origin brought oxygen into the reservoir, which oxidized sulfur-bearing products, with the final transformation to sulfuric acid. The latter in turn acts on rock-forming minerals, leaching several elements, including aluminum, iron, and calcium. Already acidified solutions are transported onto the ground surface, and hydrolysis at elevated temperatures results in forming jarosite minerals, as well as ferricopiapite. When iron sulfates begin to form, the environment of discharging solutions becomes unfavorable for zeolite formation, and the composition of the mineral association is converted to the opposite; deposits are formed that are characteristic of waters with subacid or acid pH. These deposits are similar to those discharged in zones of sulfuric acid leaching in thermal fields.

A thermal field showing strong steam–gas activity is forming at the place of Crater 022+. Table 2 shows the composition of the solutions discharged in 2023 from a small explosion crater that had preceded the formation of Crater 022+. These solutions include sodium chloride water, as well as containing potassium, calcium, ammonium, magnesium and other sulfates. The environment of the solutions is acid. Increased concentrations of arsenic (3.1 ppm) and mercury (0.00008 ppm) were observed.

4.4. Petrologic Characteristics of Igneous Rocks

Crater 022+ was found to contain exposures of fresh volcanic rocks (Fig. 5a), with fragments of similar rocks being also scattered about outside the crater along its perimeter. A description of three polished sections from a dike #178? (see Fig. 5c) (one polished section) and of the scatter along the perimeter of Crater 022+ (two polished sections) is given below.

All polished sections show similar fresh vitreous rocks. The basis is brown acid volcanic glass. The rock structure is taxitic; it is due to a combination of spots and bands of naturally occurring glasses that differ in appearance. One can discern fluidal and homogeneous glasses; microporous and comparatively compact ones; overall, there is a slight predominance of homogeneous porous and fluidal compact glasses. The glasses contain crystal clasts and small hypidiomorphic subphenocrysts of plagioclase (Pl), clinopy-

Table 4. The composition of siliceous deposits ("silicate snow") around well 022 in 2022

#	SiO_2, %	TiO_2, %	Al_2O_3, %	Fe_2O_3, FeO, %	CaO, %	MgO, %	Na_2O, %	K_2O, %	LOI	S, %
1	87.8	0.029	0.26	0.13	0.14	0.15	0.499	0.34	10.0	0.66
2	89.9	0.018	0.75	0.11	0.27	0.13	0.557	0.42	7.7	0.08

LOI means loss on ignition.

(a)

(b)

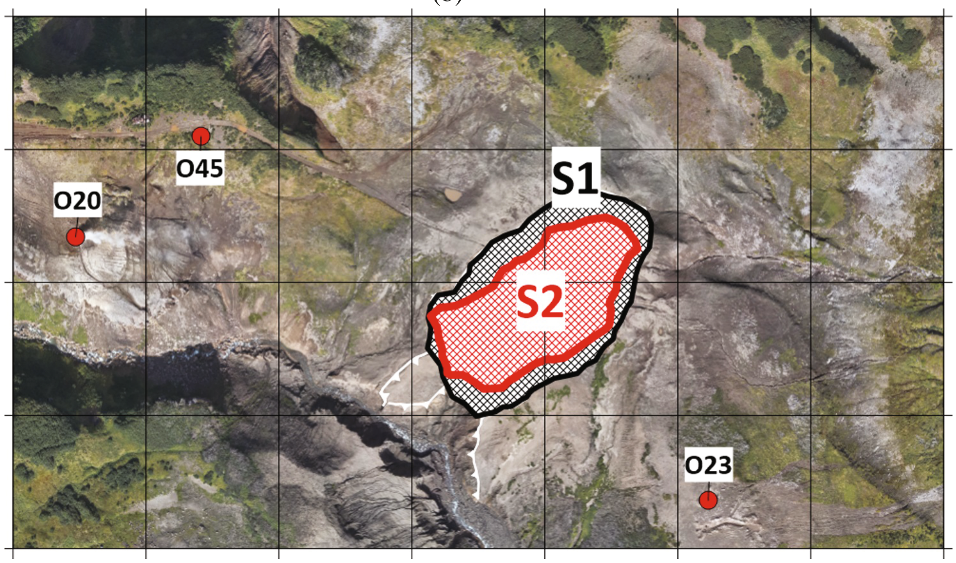

Fig. 5. Crater 022+. (a) crater of hydrothermal explosion with volume 0.29–0.36 million m^3 at the place of well 022 in the Mutnovsky geothermal field (photographed by I.A. Nuzhdaev on September 15, 2024), the crater bottom is seen to contain gypsum siliceous deposits formed by hydrothermal steam discharge; (b) S1 contour along the perimeter of the main crater produced by the hydrothermal explosion, S2 contour of the hydrothermal alteration field at the base of the explosion crater (see subsection 4.4), tick marks are at intervals of 100 m; (c) orthophoto of Crater 022+ (I.A. Nuzhdaev, September 15, 2024), unfilled black circle marks the exposure of fresh volcanic rocks (outcrop of dike #178?), a description is in main text, tick marks are at intervals of 100 m; (d) infrared survey of Crater 022+, size is in accordance with Fig. 5b, tick marks are at intervals of 100 m (I.A. Nuzhdaev, September 15, 2024).

roxenes and orthopyroxenes (Cpx, Opx), and segregations of the ore mineral (Mt). Plagioclase (Pl) phenocrysts have a composition like that of oligoclase, that is, they are acid andesines. The microstructure of the groundmass is hyaline and hypohyaline with rare microlites of acid plagioclase. One notes the presence of accessory apatite (Ap) and zircon? (Zr). Apart from crystal clasts, the glasses are found to contain not infrequent fragments of volcanic rocks with different textures and with varying degrees of freshness. Overall, up to 10% vol of these are (1) autofragments, i.e., fragments of compact fluidal glasses in porous homogeneous, or the reverse situation, the latter in the former; (2) small fragments of fresh effusive rocks with different structure (with different rock structures: aphyric, porphyritic with glomerogrowths and groundmass (hyalopilitic, trachytoidal etc.); (3) altered, recrystallized rocks.

The vitreous rocks in the three polished sections are very similar, slightly differing among themselves in quantitative relationships among kinds of glasses, phenocrysts, and varieties of volcanics in xenofragments.

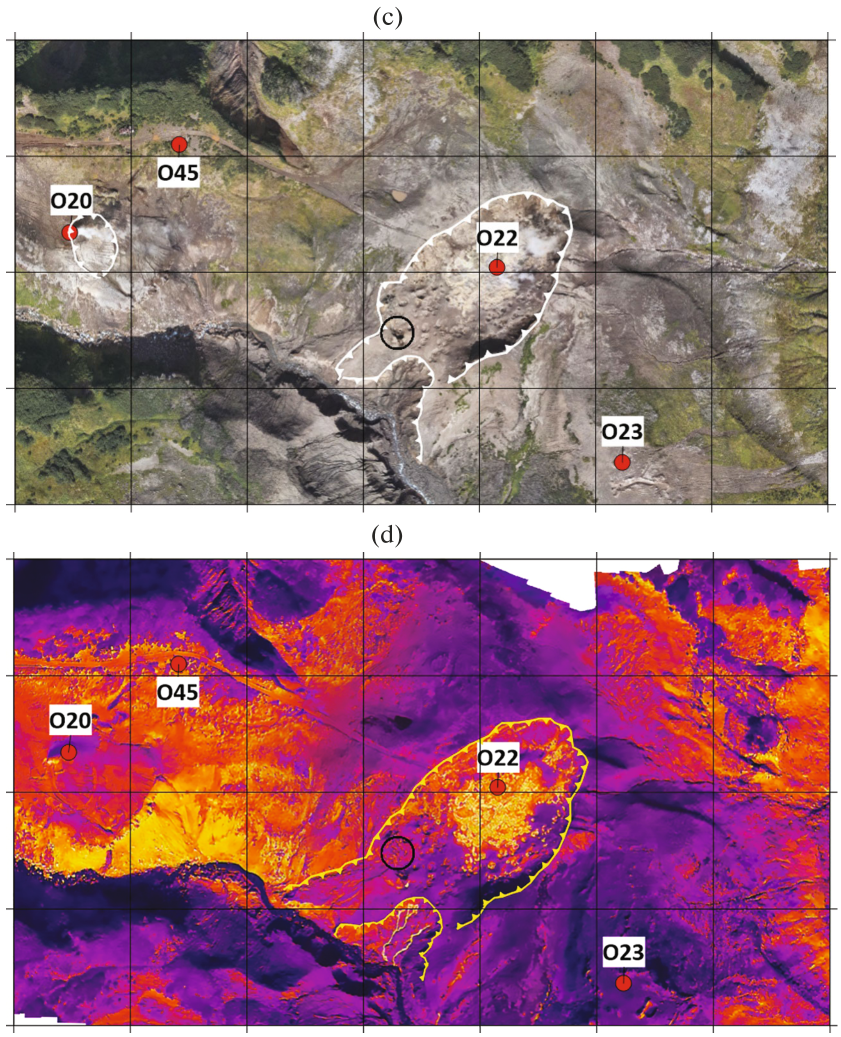

Fig. 5. (Contd.)

Taking into account the compositions of rock-forming glasses, the oligoclase composition of the plagioclase subphenocrysts, an absence of quartz in the rock; treating bipyroxene varieties in fragmental inclusions as cognate intermediate-acid/acid lavas, one can in a preliminary way name this rock hyalodacite. Taking into account the flow-about of existing vitro-crystal clasts with fluidal glass, i.e., a combination of fragmental and fluidal composition that is characteristic of welded tuffs, one can also hypothesize that fragments of ignimbrites of dacitic composition have been brought to the ground surface.

We wish to note, in the context of an incipient seismogenic fissure and its filling with magmatic fluid (dacitic melt + gas + water) containing fragments of host rocks, that in the case of high gas saturation, a dacitic melt retains high mobility, hence can form long lava flows and infill dikes (Ponomareva and Tsyurupa, 1985; Persikov and Bukhtiyarov, 2013; Persikov, 2020), including the situation with a pyro-lithoclastic termination. In particular,"pumice hills" have been mapped at the ground surface within the Mutnovsky geothermal field west of the northern test area where waste fluid is reinjected (well 028), as well as an obsidian stock (well 042), the Dachnyi and Medvezhy fumarolic fields originating in explosion craters with a pumice-litho-clastic circumference. The end of Mutnovsky-3 activity is recorded by the extrusion of a dacite dome whose age is estimated appropxmately as 4000 years based on local tephrostratigraphic data (Selyangin, 1993), diorite dikes have been crossed by drilling three wells in the Mutnovsky geothermal field, which provides an overall evidence in favor of magma injections of dioritic composition from magma system of Mutnovsky Volcano. When the feeding dike and Crater 022+ were being formed, it is also not to be ruled out that lithoclastic fragments might be captured in the upper section, including ignimbrite fragments.

5. REMOTE MONITORING OF THE FORMATION OF CRATER 022+

5.1. Using Drones

The newly formed Crater 022+ was surveyed on September 15, 2024 using a DJI Mavic 3T quadcopter equipped with wide-angle and thermovision cameras. The specifications of the quadcompter can be found at (https://aeromotus.ru/product/dji-mavic-3-thermal/). High oblique photographs and video records in visible and infrared range have been made, as well as a vertical survey at various heights. The resulting images were processed using the Agisoft Metashape Professional software. The processing yilded orthophotos of the Crater 022+ area in visible and infrared ranges (see Figs. 5a–5d). The dimensions of the resulting Crater 022+ are 200×120 m (striking northeast), the maximum depth is 30 m, with a 65 × 40-m crater being adjacent to it to the southwest (which also strikes northeast) (see Fig. 5c). The crater bottom contains numerous minor craters between 0.5 and 10 m across. The area along the perimeter of the main crater is estimated as $S1 = 17700\ m^2$, the area of the crater base over the area where minor craters occur and the area of hydrothermal alteration is estimated as $S2 = 10900\ m^2$, with mean depth (h) from 20 to 25 m, the volume of the main explosion crater (V) is estimated as lying between 0.29 and 0.36 million m^3 ($V = 0.5 \times (S1 + S2) \times h$) (see Fig. 5b). Violent steam–gas activity is occurring in the central part. Two creeks with water temperature 53°C are discharged at the southwestern boundary of the crater (see Fig. 5d).

5.2. The formation of Crater 022+ as Inferred from Satellite Observations

The fitst substantial steam explosion near well 022 took place in June 2003 (personal communication by the hydrologist L.K. Moskalev at *Geoterm* Ltd.). The new thermal field near well 022 was named *Novye 2003* (Kiryukhin et al., 2010, 2014). Melnikov (2004) analyzed satellite images (TERRA satellite with an ASTER sensor) to conclude that the explosion must be dated between April and November 2003, although this author himself dates the explosion, without giving any reasons, for late October—early November 2003. The explosion crater about 50 m across and 2 m deep was 20 m east of the head of well 022. Boiling mudpots were formed on the crater bottom, the creek that drained them had temperature 55°C, the chemical composition of its water was similar to that in well 022 based on subsequent sampling of the well (see Table 2). The attempt to close well 022 by pumping 40 m^3 of cement has not been a success, because the cement was driven by pressure back from the well onto the ground surface (I. Abkadyrov, 2024, personal communication). Well 022 had been freely blowing from 2014 through 2021, and in 2022 the wellhead control-valve was closed.

A new crater due to a hydrothermal explosion was discovered in August 2023. The crater was 1.5 m deep and about 60 m across. As reported by the Director of the Mutnovsky GeoPP, M.L. Bezotechestvo, the explosion took place in March–April 2023. An analysis of satellite images (Sentinel-2 L1C) showed that there were no signs of thermal anomalies and discharged explosion material on the snow around well 022 from October 2022 through the end of March 2023. However, the image taken on April 27, 2023 distinctly shows a 110 × 40-m heated area in snow elongate NNE and widening to reach 80 m in its southern part; the area corresponded with the location of the explosion crater (Fig. 6, image of April 27, 2023).

A new crater was found in July 2024 at the place of the 2023 explosion crater. The new crater was 200 × 120 m and as deep as 30 m, its volume was about 0.29–0.36 million m^3 (see subsection 5.1). The chronology of its formation based on an analysis of Sentinel-2 L1C imagery is as follows (see Fig. 6): (1) the December 23, 2023 image shows a displacement of the thermal anomaly by ≈50 m (to the west and south) compared with April 27, 2023; (2) the January 7, 2024 image shows an increasing degree of heating within the preceding contour; (3) the February 26, 2024 image shows an explosion hurling material east of the boundary of the actual Ctater 022+ in the form of three black flows; (4) the March 7, 2024 image already shows four black flows with higher intensity of color and dimensions; (5) the March 22, 2024 image does not show any discharges beyond the contour of the actual Crater 022+; (6) the April 6, 2024 image shows that the anomaly retains the size of the preceding image, the anomaly decreases in intensity.

Keeping in mind the above, one can suppose that the largest explosion that has formed the actual Crater 022+ occurred between February 26, 2024 and March 7, 2024.

6. A GEOMECHANICAL ANALYSIS OF THE CONDITIONS OF THE HYDROTHERMAL EXPLOSION THAT HAS PRODUCED CRATER 022+

Figure 7 shows steam hydroostatic pressure vertical profile Pp in the well (the vertical blue line), fluid pressure vertical distribution in the two-phase production geothermal reservoir geothermal reservoir PS(T) (the red line), the vertical stress Sv and the maximum horizontal SHmax stress (the black lines) vary in relation to depth for the conditions prevailing in the Mutnovsky geothermal field. The horizontal axis at bottom shows boiling temperature (saturation point) corresponding to the pressure along the horizontal axis at top.

As the steam/water level deccline in the two-phase (steam + water) productive reservoir during the operation of the Mutnovsky geothermal field (which is estimated 0.67 bar/yr or 6.7 m/year for the 20 years of

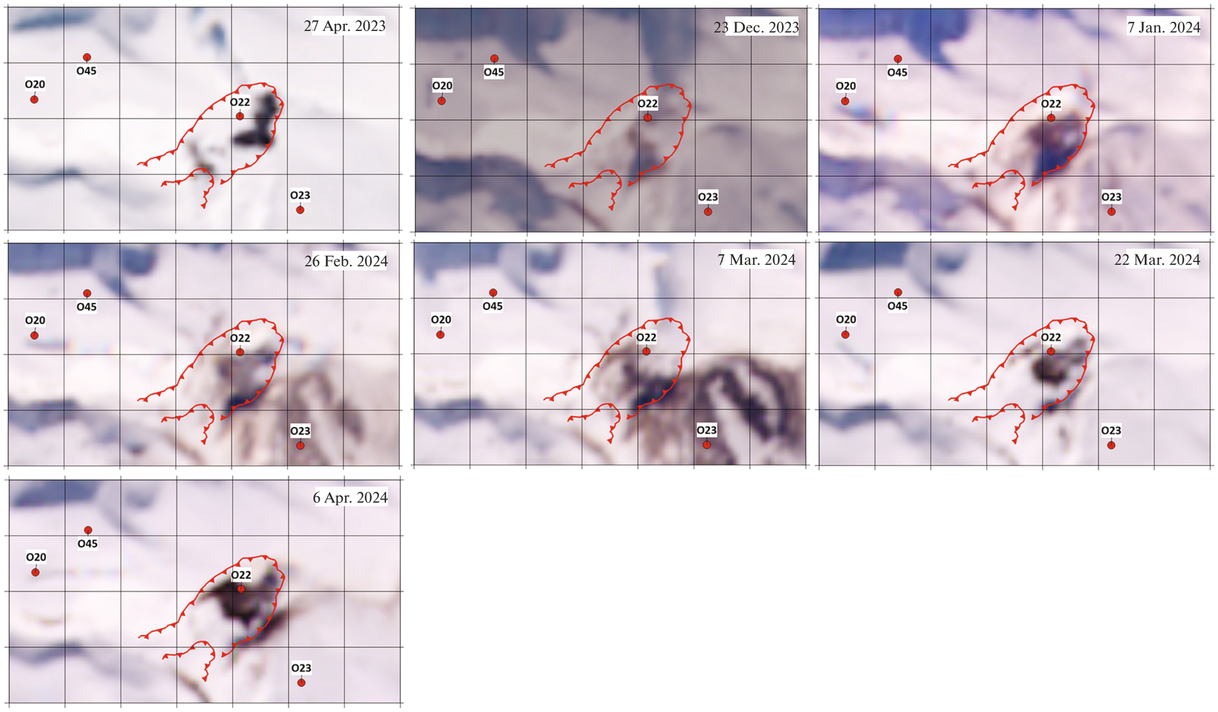

Fig. 6. The chronology of the formation of Crater 022+ as inferred from satellite images (data source is Copernicus Sentinel-2 Collection 1 MSI Level-1C (L1C) // Copernicus Data Space Ecosystem https://browser.dataspace.copernicus.eu). Note. Image size and tick marks, drawn contours of explosion craters are in agreement with Fig. 5c.

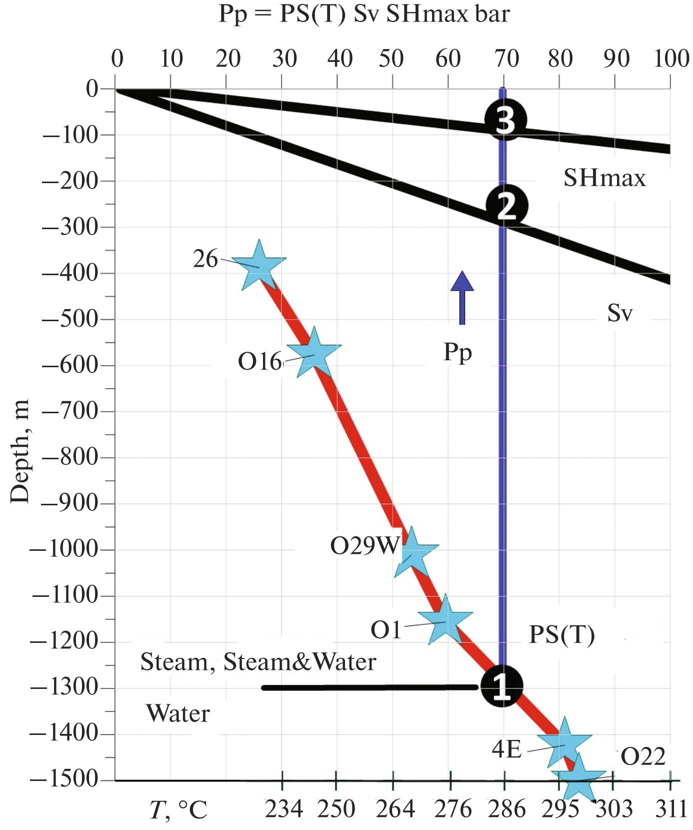

Fig. 7. A schematic mechanism of hydrothermal explosion. Stars mark data on pressure (temperature) in productive zones of respective wells; stresses Sv, SHmax as functions of depth are given for the geomechanical conditions of horizontal compression (in the Mutnovsky geothermal reservoir the conditions of horizontal compression are largely supported by low angles of dip (20–40 deg) in strike slip seismogenic faults (Kiryukhin, 2020, Fig. 4.17)).

production (Kiryukhin et al., 2018, Fig. 5), the level of thermal waters descend to the zone of higher temperatures (see Fig. 7, point 1). As a result, wellhead pressure can increase in a geothermal well closed by the wellhead cotrol-valve. As the pressure further increases to exceed the strength of the lock valve or the insulation of the conductor, the well explosion take place (see Fig. 7, line 1–3).

Strong magmatic activity in the northeastern sector of Mutnovsky Volcano (Kiryukhin at al., 2022, Fig. 10), with the dike orientation coinciding with that of productive faults in the Mutnovsky geothermal field, can be accompanied by the formation of fissures that traverse the productive two-phase geothermal reservoir and productive wells. The pressure in the *open fissure—geothermal well* system will be controlled by the maximum temperature in the two-phase geothermal reservoir (see Fig. 7, line 1–3). The potential conditions for hydrothermal explosions of the wells remain the same: pressure increasing above the strength of the lock valve or of the insulation of the conductor.

Both of the above factors for creating conditions for hydrothermal explosions of closed wells are in force in the Mutnovsky geothermal field.

Well 022 was exploded to produce a crater of volume 0.29–0.36 million m^3.

The schematic diagram for the most likely scenario of a hydrothermal explosion at the place of the blowing well 022 producing Crater 022+ seems to be the following (see Fig. 7).

(1) A dike going from the magmatic system of Mutnovsky Volcano (see Fig. 2, emplacement starting on March 4, 2024, the range of depths from –2 km to +1 km, the dip angle was 58°, dip azimuth 127°) traversed the wellbore 022 above its bottom (see Fig. 7, point 1).

(2) If the temperature at point 1 corresponds to the averaged temperature in the Mutnovsky productive geothermal reservoir (286°C), then the pressure Pp = 70 bars is strictly determined by the conditions of the two-phase reservoir state (see Fig. 7, the horizontal axes show both the pressures and the corresponding temperatures).

(3) Pressure in a vapor-dominated system is transmitted vertically without noticeable loss, so that we come from point 1 to point 2 at a depth of 250 m with the same pressure Pp = 70 bars (see Fig. 7), here the plot of Pp intersects the dependence of vertical stress Sv on depth, hence when Pp > Sv + Co, where Co is tensile strength, for tuffs it is ≈15–30 bars (Zoback, 2010) a hydraulic fracture can occur producing horizontal fissures beyond the well, if its casing column is not sufficiently sealed. The contours of the horizontal fissures produced by a hydraulic fracture determine the contours of the subsequent field of boiling springs at the base of the crater that was created by a hydrothermal explosion (in the case of Crater 022+ this is the area S2 ≈ 11 thousand m^2, see Fig. 5b).

(4) At point 3 at a depth of 80 m where the fluid pressure Pp exceeds the maximum horizontal stress SHmax (plus Co), a hydraulic frcature becomes possible both in the horizontal and in the vertical plane, i.e., a 3D failure in rock occurs, thats mean a hydrothermal explosion took place.

7. CONCLUSIONS

1. Mutnovsky Volcano for the last 4 kY ago is characterized by predominantly magmatic activity in the northeastern sector, the result being the Mutnovsky geothermal field. Dike injections can be identified using the Frac-Digger method based on seismic data reported by the KB FRC UGS RAS. In particular, in 2014–2020 a sequence of six shallow dikes striking NE has been identified, the dip was SE (from 20° to 50°) (Kiryukhin et al., 2022, Fig. 10) with the injection of another dike in early March 2003 that extended to the southern test site where wells 020, 022, and 023 are blowing. Simultaneously with its emplacement the largest hydrothermal explosion occurred with epicenter at well 022, the volume of the resulting crater was 0.29–0.36 million m^3 (Crater 022+). The fragments of unaltered volcanic rocks found at the place of the explosion might be derivates of the actual magma reservoir of dioritic composition beneath Mutnovsky Volcano or else lithoclastic ignimbrite fragments from the upper section. The hydrothermal explosion was preceded and accompanied by anomalies of pressure increase for uncondensing gases at the Mutnovsky GeoPP.

2. The mechanism of the hydrothermal explosion resulting in the formation of Crater 022+ can be explained by the fact that the dike or its gas-charged lithoclastic head traversed the wellbore 022. This resulted in transmission of steam pressure to wellhead 022 with the closed control-valve and to the shallow subhorizontal hydrothermal reservoir adjacent to the well at depths of 20–25 m. As the pressure was increasing in this reservoir, 3D fracturing occurred following the principle of hydraulic fracture with subsequent explosive output of material.

3. The bottom of the crater has a horizontal area of about 11 thousand m^2, the depth was 20–25 m; it is manifested at the surface of the explosion base by numerous small craters 1 to 10 m across, it is filled with products of hydrothermal alteration characteristic of alkaline thermal waters (opal, zeolites), after the explosion it assumed the mode of steam–gas discharge and sulfuric acid leaching. It is not ruled out that analogous subhorizontal reservoirs may exist with the potential of hydrothermal explosion beneath well 022 at greater depths.

4. Potentials for hydrothermal explosion are available (apart from Crater 022+) for wells 020, 023, and 035 in the zone of Mutnovsky Volcano magmatic activity, as well as for well 01 where temperature 264°C

was recorded at wellhead in 2008 corresponding to the pressure of saturated steam 50 bars.

5. Since the southern test site of the Mutnovsky geothermal field is envisaged to have the maximum electrical output at 25 MW (Mutnovsky GeoPP-2), theoretical and experimental work is required in order to test various scenarios for enhancing operation safety, including: (1) injection of cold water or waste fluid to condensate shallow vapor-dominated (explosion-prone) reservoirs, (2) using a geomechanically substantiated directed drilling for industrial exploitation of the zone of magmatic activity in the northeastern sector of Mutnovsky Volcano, (3) reconsider a full scale reinjection of waste fluid from Mutnovsky GeoPP into production geothermal reservoir.

6. Monitoring the seismicity of Mutnovsky Volcano and the gas concentration in heat-carrying fluid at the Mutnovsky GeoPP on-line, regular remote aerial photographing and thermal surveys (satellite imagery and drone-borne), hydrogeological sampling of blowing wells and naturally occurring thermal occurrences, are all of them effective tools for assessing the volcano's magmatic activity to ensure operation safety in the Mutnovsky geothermal field (Eichelberger et al., 2020).

ABBREVIATIONS AND NOTATION

AC	Analytical Center
FEB	Far East Branch
GIN	Geological Institute
GS	Geophysical Survey
IVS	Institute of Volcanology and Seismology
KB	Kamchatka Branch
P ncg	Pressure of noncondensing gases
RAS	Russian Academy of Sciences
RC	Resource Center
XRDMA	X-Ray Diffraction Methods of Analysis

ACKNOWLEDGMENTS

We are grateful to the Director of the *Vozobnovlyaemaya Energiya* Branch of *Kamchatskenergo* Ltd. A.A. Lyubin and the director of the Mutnovsky GeoPPs M.L. Bezotechestvo, to the leading hydrogeologist N.A. Romanov for his support of field surveys at the Mutnovsky geothermal field and for lending us data on the variation of pressure and temperature at the comdenser of the Mutnovsky GPS, to I.V. Tokarev (RC RDMI of the St. Petersburg University Science Park) for doing work in the analysis of isotopic water composition for the project no. AAAA-A19-119091190094-6, to V.Yu. Lavrushin and B.G. Pokrovsky for analyses of isotopic composition of carbon in the gas phase. We thank the reviewers for constructive remarks which have helped toward improving this paper.

This work was done using data acquired at the unique scientific installation "Seismic Infrasound Complex for Monitoring the Arctic Cryolitic Zone and a Complex for Continuous Seismic Monitoring of the Russian Federation, Adjacent Territories, and the World" (https://ckp-rf.ru/usu/507436/).

FUNDING

This work was supported by the grant of the Russian Science Foundation no. 23-27-00127, https://rscf.ru/project/23-27-00127/.

CONFLICT OF INTEREST

The authors of this work declare that they have no conflicts of interest.

REFERENCES

Akasaka, C., Takizawa, K., Todaka, N., Iwasaki, O., Tezuka, S., Nakanishi, S., Shimizu, I., and Kumazaki, N., Restoration from a large scale steam explosion at the well site of the Onikobe Geothermal Power Station, *Proceedings World Geothermal Congress 2015,* Melbourne, Australia, 19–25 April 2015.

Browne, P.R.L. and Lawless, J.V., Characteristics of hydrothermal eruptions, with examples from New Zealand and elsewhere, *Earth-Sci. Rev.,* 2001, vol. 52, pp. 299–331.

Eichelberger J., Kiryukhin A., Mollo S. [et al.] Exploring and modeling the magma–hydrothermal regime // *Geosciences* (Switzerland). 2020. Vol. 10, No. 6. P. 1–6. https://doi.org/10.3390/geosciences10060234

Fournier, R.O., Application of water chemistry to geothermal exploration and reservoir engineering, in *Geothermal Systems. Principle and Case Histories,* Rybach, L. and Muffler, L.J.P., Eds., N.Y.: J. Wiley, 1981, pp. 109–143.

Friðleifsson, G, Pálsson, B., Albertsson, A., Stefánsson, B., Gunnlaugsson, E., Ketilsson, J., and Gíslason, P., IDDP-1 drilled into magma—World's first magma-EGS system created, in *Proceedings World Geothermal Congress 2015* Melbourne, Australia, 19–25 April 2015.

Gudmundsson, A., How local stresses control magma-chamber ruptures, dyke injections, and eruptions in composite volcanoes, *Earth-Sci. Rev.,* 2006, vol. 79, pp. 1–31.

Gudmundsson, A., The propagation paths of fluid-driven fractures in layered and faulted rocks, *Geological Magazine,* 2022, vol. 159, pp. 1978–2001. doi.org/ https://doi.org/10.1017/S0016756822000826

Kiryukhin, A.V., High temperature fluid flows in the Mutnovsky hydrothermal system, Kamchatka, *Geothermics,* 1993, vol. 23, no. 1, pp. 49–64.

Kiryukhin, A.V., Modeling studies: The Dachny geothermal reservoir, Kamchatka, Russia, *Geothermics,* 1996, vol. 25, no. 1, pp. 63–90.

Kiryukhin, A.V., *Geotermoflyuidomekhanika gidrotermalnykh, vulkanicheskikh i uglevodorodnykh sistem* (Geothermal Fluid Mechanics of Hydrothermal, Volcanic, and Hydrocarbon Systems), Ct. Petersburg: Eko-Vektor Ai-Pi, 2020.

Kiryukhin, P.A. and Kiryukhin, A.V., *Frac-Digger.* Russian Federation Inventor's Certificate no. 2016612168 for computer software as of June 21, 2016.

Kiryukhin, A.V., Kiryukhin, V.A., and Manukhin, Yu.F., *Gidrogeologiya vulkanogenov* (Hydrogeology of Volcanic Rocks), St. Petersburg: Nauka, 2010.

Kiryukhin, A.V., Asaulova, N.P., Vereina, O.B., and Polyakov, A.Yu., Estimating the influence of filtering during the operation of the Pauzhetka and Mutnovskii high-temperature geothermal fields, Kamchatka, Russia, *J. Volcanol. Seismol.,* 2014, vol. 8, no. 3, pp. 156–167.

Kiryukhin, A.V., Fedotov, S.A., and Kiryukhin, P.A., A geomechanical interpretation of the local seismicity related to eruptions and renewed activity on Tolbachik, Koryakskii, and Avacha Volcanoes, Kamchatka, in 2008–2012, *J. Volcanol. Seismol.,* 2016, vol. 10, no. 5, pp. 275–291.

Kiryukhin, A., Lavrushin, V., Kiryukhin, P., and Voronin, P., Geofluid systems of Koryaksky-Avachinsky volcanoes (Kamchatka, Russia), *Geofluids,* 2017. 4279652.

Kiryukhin, A.V., Polyakov, A.Y., Usacheva, O.O., and Kiryukhin, P.A., Thermal-permeability structure and recharge conditions of the Mutnovsky high temperature geothermal field (Kamchatka, Russia), *J. of Volcanology and Geothermal Res.,* 2018, vol. 356, pp. 36–55.

Kiryukhin, A., Chernykh, E., Polyakov, A., and Solomatin, A., Magma fracking beneath active volcanoes based on seismic data and hydrothermal activity observations, *Geosciences,* 2020, vol. 10, no. 2, no. 52. 10020052.

Kiryukhin, A.V., Polyakov, A.Y., Voronin, P.O., Zhuravlev, N.B., Usacheva, O.O., and Solomatin A.V., Magma fracking and production reservoirs beneath and adjacent to Mutnovsky Volcano based on seismic data and hydrothermal activity, *Geothermics,* 2022, vol. 105. 102474.

Kiryukhin, A.V., Polyakov, A.Yu., and Zhuravlev, N.B., Russian Federation Inventor's Certificate no. 2801789 C1, *A Device for Estimating Partial Pressure of Uncondensed Gas in a Geothermal Vapor*, August 15, 2023a.

Kiryukhin, A.V., Bergal-Kuvikas, O.V., and Lemzikov, M.V., Magmatic activity of Klyuchevskoy volcano triggering eruptions of Bezymianny volcano based on seismological and petrological data, *Journal of Volcanology and Geothermal Res.,* 2023b, vol. 442. 107892.

Melnikov, D.V., Some features in the morphology of hydrothermal explosions in the area of the Mutnovsky Geothermal Station, *Vestnik Kamch. Reg. Ass. Uch.-Nauch. Ts. Ser. Nauki o Zemle,* 2004, no. 4, pp. 120–124.

Persikov, E.S., Interrelationship between the relative crustal abundances of intrusive and effusive rocks in the acid–basic series on the one hand and patterns of magma viscosity on the other, *Geol. Geofiz.,* 2020, vol. 61, nos. 5–6, pp. 725–733.

Persikov, E.S. and Bukhtiarov, P.G., Generalized patterns in the dynamical properties of magma: Viscosity and water diffusion, *Vestnik SPb. Univ.,* 2013, Ser. 7, no. 3, pp. 50–64.

Polyakov, A.Yu. and Kiryukhin, A.V., Magmatic activity of Mutnovsky Volcano in 2009–2024, in *Materialy Vserossiiskoi nauchnoi konferentsii s mezhdunarodnym uchastiem "Geotermalnaya vulkanologiya, gidrogeologiya, geologiya nefti i gaza"* (Proc. All-Russia Conf. with international participation "Geothermal Volcanology, Hydrogeology, Petroleum Geology" (Geothermal Volcanology Workshop 2024), September 2–8, 2024, Petropavlovsk-Kamchatsky: IViS DVO RAN, 2024, pp. 16–19.

Ponomareva, V.V. and Tsyurupa, A.A., On long flows of liquid acid lava on Krasheninnikov Volcano, *Vulkanol. Seismol.,* 1985, no. 3, pp. 85–92.

Selyangin, O.B., Mutnovsky Volcano, Kamchatka: New data on the structure, evolution, and the prediction of activity, *Vulkanol. Seismol.,* 1993, no. 1, pp. 17–30.

Sergeeva, A.V., Rychagov, S.N., Kravchenko, O.V., Sandimirova, E.I., Nazarova, M.A., Kartasheva, E.V., and Kuzmina, A.A., Mineral and geochemical features of zeolite-siliceous deposits at the Pauzhetka Geothermal Field, southern Kamchatka, *J. Volcanol. Seismol.,* 2024, vol. 18, no. 1, pp. 32–47.

Simon, A., Yogodzinski, G.M., Robertson, K., Smith, E., Selyangin, O., Kiryukhin, A., Mulcahy, S.R., and Walker, J.D., Evolution and genesis of volcanic rocks from Mutnovsky Volcano, Kamchatka, *J. Volcanol. Geotherm. Res.,* 2014, vol. 286, pp. 116–137.

Stefansson, V., The Krafla geothermal field, North-Eastern Iceland, in *Geothermal Systems. Principle and Case Histories,* Rybach, L. and Muffler, L.J.P., Eds., N. Y.: J. Wiley, 1981, pp. 271–294.

Vakin, E.A., Pilipenko, G.F., and Sugrobov, V.M., A general characteristization of the Mutnovsky geothermal field and an inferred estimate of resources, in *Geotermicheskie i geokhimicheskie issledovaniya vysokotemperaturnykh gidroterm* (Geothermal and Geochemical Studies of High-Temperature Hydrothermal Occurrences), Sugrobov, V.M., Ed., Moscow: Nauka, 1986, pp. 6–41.

Translated by A. Petrosyan

Publisher's Note. Pleiades Publishing remains neutral with regard to jurisdictional claims in published maps and institutional affiliations.
AI tools may have been used in the translation or editing of this article.